ACS APPLIED MATERIALS & INTERFACES

Letter

www.acsami.org

Perovskite Solar Cell Using a Two-Dimensional Titania Nanosheet Thin Film as the Compact Layer

Can Li,[†] Yahui Li,[†] Yujin Xing,[‡] Zelin Zhang,[†] Xianfeng Zhang,[§] Zhen Li,[⊥] Yantao Shi,[‡] Tingli Ma,[‡] Renzhi Ma,[∥] Kunlin Wang,[†] and Jinquan Wei*[,†]

[†]Key Lab for Advance Materials Processing Technology of Education Ministry, State Key Lab of New Ceramic and Fine Processing, and School of Materials Science and Engineering, Tsinghua University, Beijing 100084, P. R. China

[‡]State Key Laboratory of Fine Chemicals, School of Chemistry, Dalian University of Technology, Dalian 116024, P. R. China

[§]National Center for Nanoscience and Technology, Beiyitiao 11, Beijing 100190, P. R. China

[⊥]National Renewable Energy Laboratory, Golden, Colorado 80401, United States

[∥]National Institute for Materials Science, 1-1 Namiki, Tsukuba, Ibaraki 3050044, Japan

Supporting Information

ABSTRACT: The compact layer plays an important role in conducting electrons and blocking holes in perovskite solar cells (PSCs). Here, we use a two-dimensional titania nanosheet (TNS) thin film as the compact layer in $CH_3NH_3PbI_3$ PSCs. TNS thin films with thicknesses ranging from 8 to 75 nm were prepared by an electrophoretic deposition method from a dilute TNS/tetrabutylammonium hydroxide solution. The TNS thin films contact the fluorine-doped tin oxide grains perfectly. Our results show that a 8-nm-thick TNS film is sufficient for acting as the compact layer. Currently, the PSC with a TNS compact layer has a high efficiency of 10.7% and relatively low hysteresis behavior.

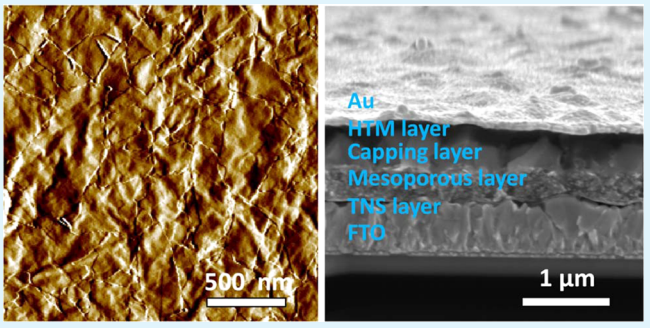

KEYWORDS: *perovskite solar cell, titania nanosheet, compact layer, electrophoretic deposition*

Organic−inorganic hybrid perovskite solar cells (PSCs) have attracted great attention since their debut in 2009.[1−5] During these years, the structure of the PSC has evolved from sensitization to a p−n junction, and the power conversion efficiency (PCE) has been improved dramatically from an initial 3.81% to 20.3%.[1,2,6] Although there might be some device configurations without a compact layer, two main components are required for most high-efficiency PSCs: active perovskite and a compact layer. The compact layer plays an important role in conducting electrons, blocking holes, and transmitting light. This requires the compact layer to have a continuous, uniform, and ultrathin structure. Generally, the compact layers were fabricated from a precursor TiO_2 nanoparticle (TNP) onto a fluorine-doped tin oxide (FTO) substrate by spin coating[7] and spray pyrolysis.[8] Because the FTO surface has a roughness of 20−30 nm, it is hard to make an ideal compact layer with uniform thickness. Furthermore, to avoid pinholes in the compact layer, the TNP film is usually required to have a thickness of ∼50 nm, which increases light absorption in the compact layer and the series resistance of the devices. Recently, thermal oxidation of a titanium thin film and atomic layer deposition were also used to prepare the compact layer with atomic thickness.[9,10] However, it is hard to scale up. Two-dimensional (2D) materials are promising for preparing uniform, atomic thick films in a large area. Up to now, there have been no reports on using 2D materials as the compact layer in PSCs.

The titania nanosheet (TNS) is one of the 2D materials, which has been introduced to photocatalysis, lithium batteries, and dye-sensitized solar cells.[11] The TNS has a wide band gap of ∼3.8 eV and a high mobility of 5×10^2 cm^2 V^{-1} s^{-1}, which make it possible to use in electronic and photovoltaic devices.[12,13] Generally, the TNS is prepared through chemical exfoliation of a layered titanate crystal.[14] By ion-exchange reactivity, tetrabutylammonium hydroxide (TBA^+) was inserted into the interlayer of a titanate crystal and formed an aqueous colloidal solution with TBA^+ as the cation and TNS as the anion. Because the TNS is negatively charged, it can be assembled into a thin film layer by layer using an electrophoretic deposition (EPD) method.[15,16] Here, we fabricated a high-quality TNS thin film in a large area from a TNS/TBA^+ colloidal solution by the EPD method, where the TNS covers the FTO grains nearly perfectly. PSCs using the TNS as a compact layer were then investigated.

Figure 1a is an atomic force microscopy (AFM) image of the TNS film prepared by dropping a few drops of a TNS/TBA^+

Received: March 4, 2015
Accepted: July 6, 2015
Published: July 6, 2015

DOI: 10.1021/acsami.5b01959
ACS Appl. Mater. Interfaces 2015, 7, 15117−15122

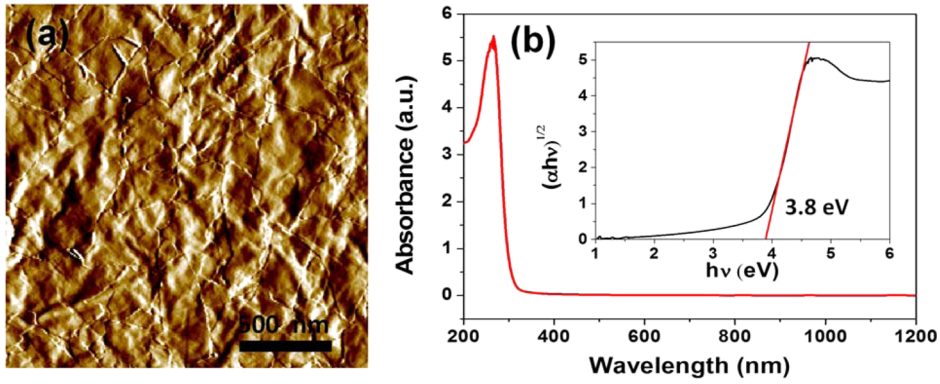

Figure 1. (a) AFM image of the TNS depositing onto a SiO_2/Si substrate. (b) UV−vis−near-IR absorption spectrum of the TNS solution. Inset: Plot of $(\alpha h\nu)1/2$ versus $h\nu$ showing an optical band gap of 3.8 eV.

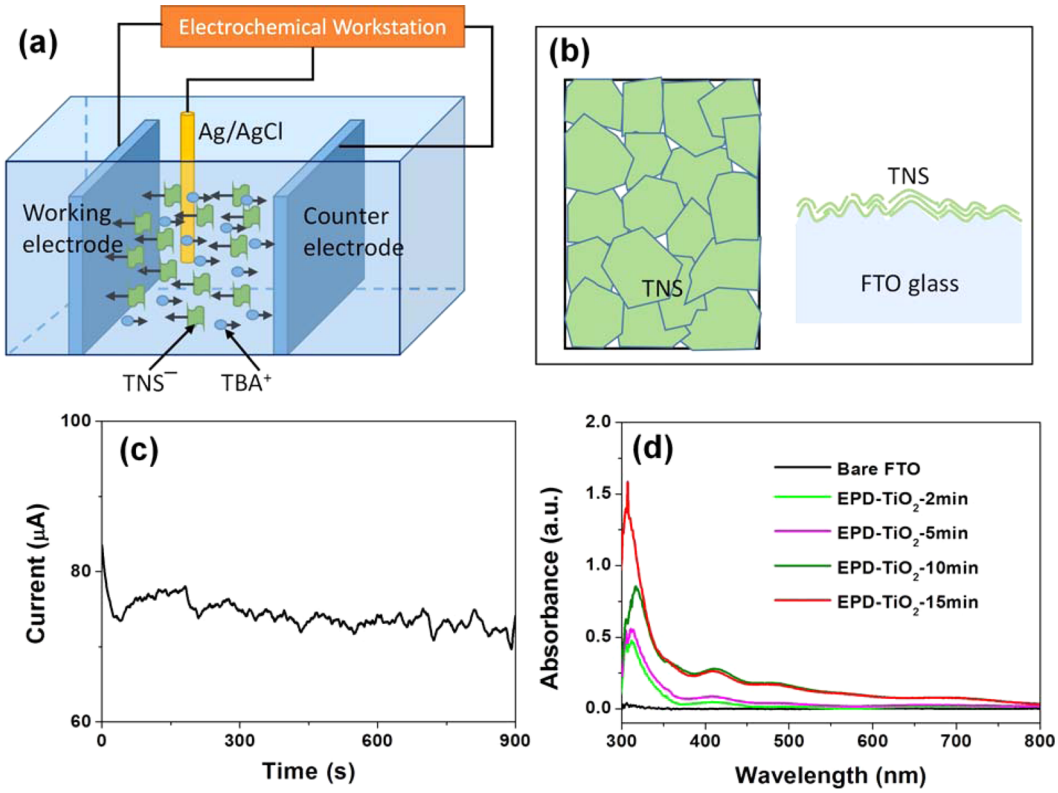

Figure 2. (a) Schematic diagram of the EPD process of the TNS. (b) Schematic diagram of the TNS depositing on the FTO glass. (c) Plot of the deposition current versus time. (d) UV−vis absorption spectra of the TNS film prepared by different EPD times.

solution onto a SiO_2/Si substrate. The TNS self-assembles to a continuous film. The TNS edges can be clearly identified. The TNS has a lateral size of 0.2−2 μm and a thickness of 1−3 nm. Figure 1b shows an absorbance spectrum of a dilute TNS aqueous solution, showing a strong absorption peak at ~270 nm and an ultralow absorption in the visible region. The inserted graph in Figure 1b shows that the TNS has an optical band gap of 3.8 eV, which is consistent with the value reported previously.[12]

Figure 2a shows a schematic diagram of the EPD process. The TNS/TBA^+ solution was diluted to 40 mg L^{-1} in ethanol. When a working voltage of 10 V is applied, the TNS moves to the working electrode, while TBA^+ moves to the counter electrode. As illustrated in Figure 2b, the TNS covers the FTO substrate and they overlap each other. There might be some tiny holes in the TNS thin film at the beginning of deposition. The holes will be patched by the TNS quickly. Because of the atomic thickness and high flexibility, the TNS can cover and contact the FTO grains easily (see the right side of Figure 2b). Because of the high electrical resistance of the TNS, the deposition current changes during the EPD process. Figure 2c shows a typical deposition current versus time curve. It is clear that the current declines sharply at the first 40 s of the EPD, which derives from deposition of the TNS. It can be deduced that the FTO surface is fully covered by a continuous TNS film in 40 s. As the EPD time is extended, the thickness of the TNS film increases gradually. There are current fluctuation during the EPD, which derives from gas (O_2 and H_2) bubble generation at high potential (10 V). When the bubbles break, the TNS film will partially break, leading to an increase of the deposition current. The TNS will patch the broken area quickly, resulting in a decrease of the deposition current.

DOI: 10.1021/acsami.5b01959
ACS Appl. Mater. Interfaces 2015, 7, 15117−15122

Figure 2d shows absorption spectra of the TNS thin films prepared by various EPD times. The bare FTO substrate was used for baseline correction. As shown in Figure 2d, the TNS thin films prepared by short-time EPD (≤5 min) have very low absorbance in the visible region. When the EPD time exceeds 10 min, the absorbance of the TNS thin film increases evidently. This indicates that the light harvest of solar cells will be affected by the deposition time.

Figure 3a shows a tilt-viewed scanning electron microscopy (SEM) image of the TNS thin film on the FTO substrate at the initial stage of deposition (EPD time: 30 s). It is clear that the TNS covers the FTO grains very well, which results in a wavy TNS film. It is noted that there might be pinholes in some samples prepared by short-time EPD (see Figure S1 in the Supporting Information, SI). Figure 3b shows a top-view SEM image of a TNS film prepared by 5 min of EPD. This shows a continuous, uniform, and high-quality TNS thin film on the FTO substrate. The TNS thin film is highly transparent, through which the FTO grains are observed clearly. This indicates that the interface between the TNS and FTO surface is quite good for short-time (≤5 min) deposition. Parts c–f of Figure 3 show cross-sectional SEM images of the TNS films prepared at different EPD times. The TNS thin films have uniform thickness for all samples. The thicknesses, measured by SEM under high magnification (see Figure S2 in the SI), are 8, 14, 43, and 72 nm for samples prepared at EPD times of 2, 5, 10, and 15 min, respectively. The thickness of the TNS thin film increases almost linearly with the EPD time (see Figure S3 in the SI). The TNS film with a thickness of less than 20 nm has a good interface with the FTO substrate. However, for the thick TNS film, it might be peeled off under stress (see Figure 3f). For comparison, we also prepared a TNP thin film on the FTO substrate by a spin-coating method. The morphology of the TNS film is quite different from that of the TNP layer (see Figure S4 in the SI). It has a perfect interface between the TNP and FTO substrate. Because of the rough FTO surface, the TNP film has a smooth surface and a nonuniform thickness, while the TNS thin film has a rough surface and a uniform thickness.

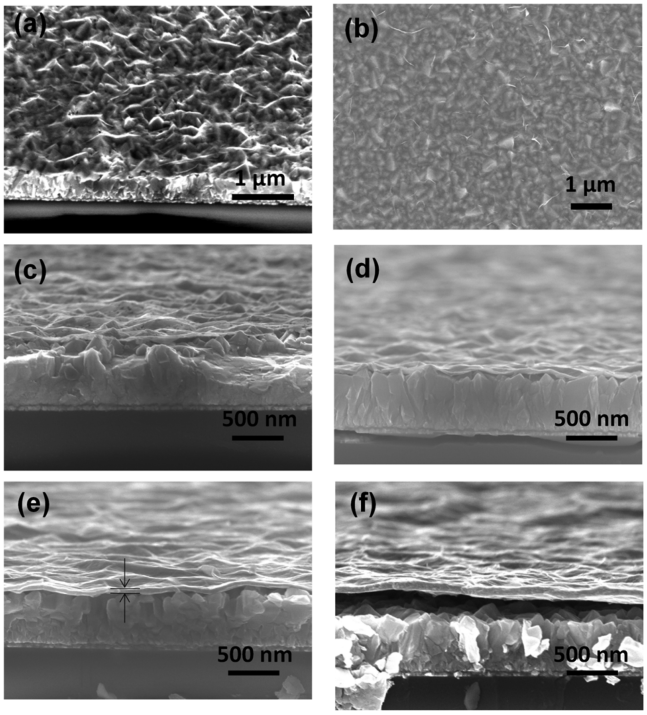

Figure 3. SEM images of the TNS depositing on the FTO glass. (a) Tilted-view (45°) SEM image at an initial deposition stage (EPD time: 30 s). (b) Top-view image of the TNS thin film (EPD time: 5 min). (c–f) Side-view images of the TNS film prepared at EPD times of 2, 5, 10, and 15 min, respectively.

We fabricated $CH_3NH_3PbI_3$ PSCs through a two-step method according to the literature[17] using the TNS as a compact layer. As shown in Figure 4a, the PSC consists of a FTO substrate, a TNS compact layer, a mesoporous layer, a $CH_3NH_3PbI_3$ perovskite capping layer, a hole-transport layer, and a gold back-electrode. The device has a good interface between the TNS layer and FTO, as well as the TNS and the mesoporous layer. For comparison, PSCs with a TNP compact layer are also fabricated by the same method. The TNP layer has an average thickness of 50 nm (see Figure S5 in the SI). Figure 4b shows a SEM image of the $CH_3NH_3PbI_3$ capping layer. The $CH_3NH_3PbI_3$ perovskite has grain sizes ranging from 200 to 500 nm and some holes (as shown by arrows) among the grains. Figure 4c is an X-ray diffraction (XRD) plot of the $CH_3NH_3PbI_3$ capping layer. The XRD peaks are consistent with those reported recently.[18,19] Although there is some residual PbI_2 in the sample, the $CH_3NH_3PbI_3$ perovskite is well crystallized.

Figure 4d shows light and dark current density–voltage (J–V) curves of PSCs using a ∼15 nm TNS thin film (EPD time: 5 min) and TNP as a compact layer, respectively. The dark J–V curves of both cells give nearly ideal rectification performances. This indicates that the TNS thin film can act as an ideal compact layer. The PSC with a TNS compact layer shows a PCE of 9.8% with an open-circuit voltage (V_{oc}) of 979 mV, a short-circuit current density (J_{sc}) of 16.8 mA cm^{-2}, and a fill factor (FF) of 0.59, respectively, which are slightly higher than those using TNP as a compact layer (PCE = 9.3%, V_{oc} = 964 mV, J_{sc} = 17.1 mA cm^{-2}, and FF = 0.56). It is noted that the PCEs of the solar cells using both TNS and TNP as compact layers are not so high. We believe that the relatively low PCE of the solar cell derives mainly from the quality of the $CH_3NH_3PbI_3$ layer rather than from the compact layer. There is an intersection between the light and dark J–V curves at high bias voltage for both PSCs, which indicates that the recombination of the electron–hole pairs occurs in the $CH_3NH_3PbI_3$ layer.

Table 1 summarizes the photovoltaic parameters of PSCs using a TNS thin film with various EPD times as the compact layer. For comparison, the photovoltaic parameters of the solar cells using a TNP as the compact layer are also provided. Here, we use the mean value and standard deviation of the solar cells (as shown in Figure S6 in the SI) rather than the numerical average value. The PSC with a ∼15 nm TNS compact layer has an average efficiency of 9.3% and a best value of 10.7%, while the PSC with a TNP compact layer has a mean efficiency of 9.4% and a best efficiency of 10.5%. The devices with 2-min-EPD TNS thin films have the highest J_{sc} and the lowest V_{oc} and FF (see Figure S7 in the SI), which indicates that the TNS film with a thickness of 8 nm is sufficient for use as a compact layer. With a EPD time extending to 10 min, V_{oc} is maintained at 880–980 mV, while J_{sc} keeps decreasing (see Figure S7 in the SI). A decrease in J_{sc} derives from light absorption in the TNS compact layer and series resistance. As shown in Figure 2c, the absorbance of the compact layer increases as the EPD time is

DOI: 10.1021/acsami.5b01959
ACS Appl. Mater. Interfaces 2015, 7, 15117–15122

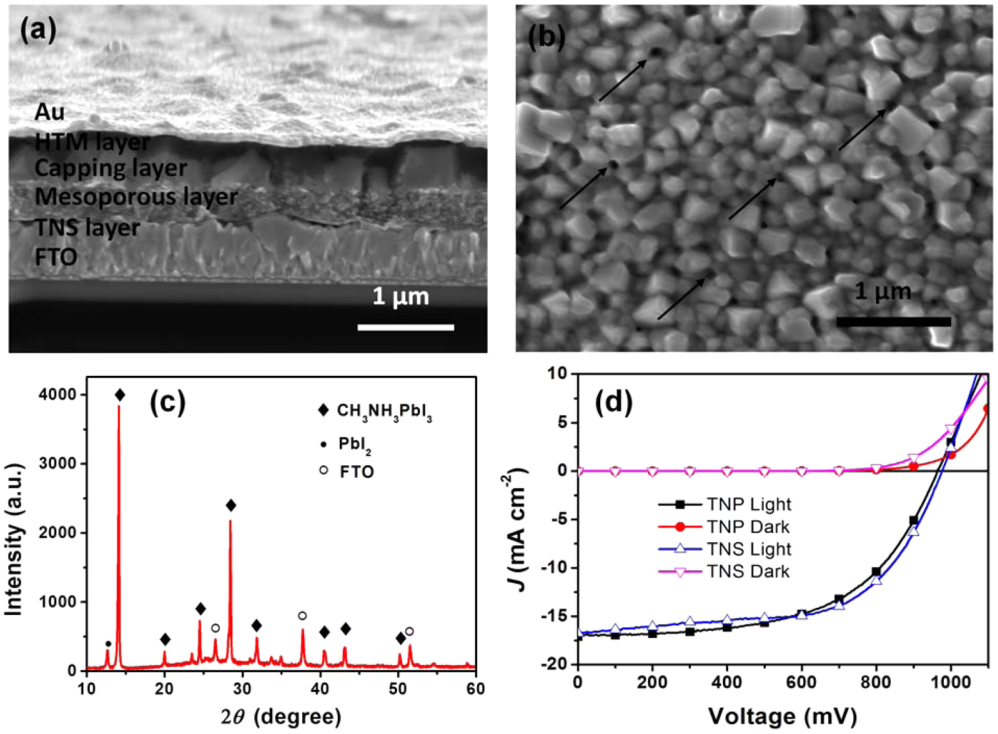

Figure 4. (a) SEM image of the $CH_3NH_3PbI_3$ solar cell using the TNS thin film as a compact layer. (b) SEM image of the $CH_3NH_3PbI_3$ capping layer. (c) XRD plot of $CH_3NH_3PbI_3$ on FTO glass. (d) Dark and light $J-V$ curves of the PSCs using TNS (open symbols) and TNP (solid symbols) as compact layers.

Table 1. Photovoltaic Properties of the $CH_3NH_3PbI_3$ PSCs Using TNS Films Made from Various EPD Times and TNP Films as Compact Layers

EPD time (min)	thickness (nm)	V_{oc} (mV)	J_{sc} (mA cm^{-2})	FF	PCE (%)	R_s (Ω cm^2)
2	8	912 ± 14	17.3 ± 1.7	0.57 ± 0.05	9.1 ± 1.2	7.0 ± 3.3
5	14	925 ± 45	16.5 ± 0.7	0.61 ± 0.03	9.3 ± 0.7	9.6 ± 4.7
10	43	925 ± 33	15.8 ± 1.0	0.61 ± 0.05	8.9 ± 1.0	9.9 ± 5.0
15	72	913 ± 29	14.9 ± 1.0	0.62 ± 0.04	8.4 ± 0.8	8.1 ± 2.9
TNP	~50	922 ± 35	18.5 ± 1.3	0.54 ± 0.02	9.4 ± 0.4	14.6 ± 6.2

extended. This indicates that less light is absorbed by the active perovskite layer for the thick compact layer. Although PSCs using ~8 nm TNS thin films as compact layers have the highest J_{sc}, it is not so stable for device fabrication because of current leakage through pinholes in some TNS thin-film samples (see Figure S1 in the SI). For a TNS thin film with an EPD time of 5 min, a uniform, continuousd and fully covered thin film is formed on the FTO substrate, which also ensures high light transmittance, resulting in a stable and high performance of the PSCs.

Hysteresis between the $J-V$ curves obtained from forward and reverse scans is a unique phenomenon in the PSCs. Parts a and b of Figure 5 show the forward and reverse scanning light $J-V$ curves of PSCs using TNS and TNP as compact layers (scan rate 100 mV s^{-1}), respectively. The corresponding photovoltaic parameters are provided in Table S1 in the SI. Evident hysteresis phenomena are observed in both cells. For the PSC with a TNS compact layer, V_{oc} and FF obtained from the forward scan are lower than those from the reverse scan. As a result, the PSC has a PCE of 9.2% in the forward scan and 10.7% in the reverse scan. For the PSC with a TNP compact layer, J_{sc} and FF in the forward scan are lower than those in the reverse scan, leading to a PCE of 8.5% in the forward scan and a PCE of 10.5% in the reverse scan. This shows that the cell with a TNS compact layer has less hysteresis effect than that with a TNP compact layer. It has been reported that many factors are responsible for hysteresis, such as the structure of PSCs,[20] the ferroelectric property and crystalline size of perovskite,[20,21] the mesoporous TiO_2 layer,[22] and the interface between the TiO_2 compact layer and the FTO substrate.[23] Because the main differences between the PSCs with TNS and TNP films are the compact layers and their interface with the FTO substrate, we investigate the hysteresis effect of the PSC by measuring the forward and reverse scan $I-V$ curves of the bare TNS (~15 nm) and TNP (~50 nm) thin film on the FTO substrate (see the inset of Figure 5c). The dark $I-V$ curve in Figure 5c shows that there is evident hysteresis between the compact layer and the FTO substrate for both TNS and TNP films. This indicates that the compact layer and its interface with FTO contribute to hysteresis in the PSCs. The current change of TNS/FTO between the forward and reverse scan is smaller than that of TNP/FTO (see Figure S8 in the SI). This might be the reason why the PSC with a TNS compact layer has a lower hysteresis effect than those using TNP as a compact layer. Figure 5d shows the dependence of the photocurrent density and PCE on time measured at 680 mV for the PSC with a TNS compact layer and at 670 mV for the PSC with a TNP

DOI: 10.1021/acsami.5b01959
ACS Appl. Mater. Interfaces 2015, 7, 15117−15122

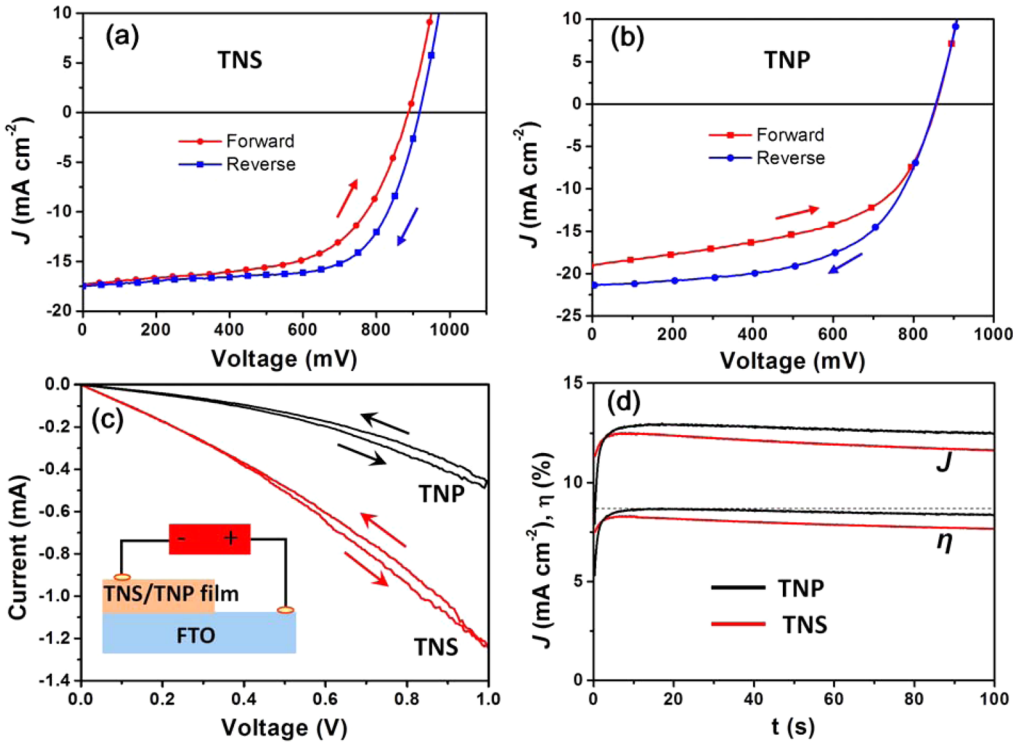

Figure 5. Light $J-V$ curves of a PSC using TNS (a) and TNP (b) as compact layers. (c) Dark $J-V$ curves of TNS/FTO and TNP/FTO. The inset schematic shows the conditions of voltage applied across the films. (d) Photocurrent density and PCE as a function of time for two cells respectively using TNS and TNP as compact layers measured at a voltage close to 0.68 V.

compact layer, respectively. The photocurrent density decays gently, leading to a decrease of PCE for both PSCs.

In summary, high-quality TNS thin films are prepared by the EPD method from a TNS/TBA^+ colloidal solution. The negatively charged TNS covers the FTO substrate perfectly. The thicknesses of the TNS thin films are well controlled by the EPD time. The TNS film with a thickness of 8 nm is sufficient to act as the compact layer in the $CH_3NH_3PbI_3$ PSCs. The PSC with a TNS compact layer has a PCE of 10.7% and a low hysteresis effect.

■ ASSOCIATED CONTENT

Supporting Information

Experimental method, thickness measurement of the TNS films, SEM images of TNP and TNS compact layers, histogram of efficiency, photovoltaic parameters of the PSCs, and hysteresis phenomenon in TNS and TNP films. The Supporting Information is available free of charge on the ACS Publications website at DOI: 10.1021/acsami.5b01959.

■ AUTHOR INFORMATION

Corresponding Author

*E-mail: jqwei@tsinghua.edu.cn.

Notes

The authors declare no competing financial interest.

■ ACKNOWLEDGMENTS

This work is financially supported by the National Natural Science Foundation of China (Grant 51172122), Tsinghua University Initiative Scientific Research Program (Grant 20111080939), and Shenzhen Jiawei Photovoltaic Lighting Co., Ltd.

■ REFERENCES

(1) Kojima, A.; Teshima, K.; Shirai, Y.; Miyasaka, T. Organometal Halide Perovskites as Visible-Light Sensitizers for Photovoltaic Cells. *J. Am. Chem. Soc.* **2009**, *131*, 6050−6051.

(2) Kim, H. S.; Im, S. H.; Park, N. G. Organolead Halide Perovskite: New Horizons in Solar Cell Research. *J. Phys. Chem. C* **2014**, *118*, 5615−5625.

(3) Kim, H.-S.; Lee, C.-R.; Im, J.-H.; Lee, K.-B.; Moehl, T.; Marchioro, A.; Moon, S.-J.; Humphry-Baker, R.; Yum, J.-H.; Moser, J. E.; Grätzel, M.; Park, N.-G. Lead Iodide Perovskite Sensitized All-Solid-State Submicron Thin Film Mesoscopic Solar Cell with Efficiency Exceeding 9%. *Sci. Rep.* **2012**, *2*, 591−597.

(4) Stranks, S. D.; Eperon, G. E.; Grancini, G.; Menelaou, C.; Alcocer, M. J. P.; Leijtens, T.; Herz, L. M.; Petrozza, A.; Snaith, H. J. Electron-Hole Diffusion Lengths Exceeding 1 Micrometer in an Organometal Trihalide Perovskite Absorber. *Science* **2013**, *342*, 341−344.

(5) Xing, G.; Mathews, N.; Sun, S.; Lim, S. S.; Lam, Y. M.; Grätzel, M.; Mhaisalkar, S.; Sum, T. C. Long-Range Balanced Electron and Hole-Transport Lengths in Organic-Inorganic $CH_3NH_3PbI_3$. *Science* **2013**, *342*, 344−347.

(6) Jeon, N. J.; Noh, J. H.; Yang, W. S.; Kim, Y. C.; Ryu, S.; Seo, J.; Seok, S. I. Compositional Engineering of Perovskite Materials for High-Performance Solar Cells. *Nature* **2015**, *517*, 476−480.

(7) Zhou, H.; Chen, Q.; Li, G.; Luo, S.; Song, T.-b.; Duan, H.-S.; Hong, Z.; You, J.; Liu, Y.; Yang, Y. Interface Engineering of Highly Efficient Perovskite Solar Cells. *Science* **2014**, *345*, 542−546.

(8) Li, Z.; Kulkarni, S. A.; Boix, P. P.; Shi, E.; Cao, A.; Fu, K.; Batabyal, S. K.; Zhang, J.; Xiong, Q.; Wong, L. H.; Mathews, N.; Mhaisalkar, S. G. Laminated Carbon Nanotube Networks for Metal Electrode-Free Efficient Perovskite Solar Cells. *ACS Nano* **2014**, *8*, 6797−6804.

(9) Wu, Y. Z.; Yang, X. D.; Chen, H.; Zhang, K.; Qin, C. J.; Liu, J.; Peng, W. Q.; Islam, A.; Bi, E. B.; Ye, F.; Yin, M. S.; Zhang, P.; Han, L. Y. Highly Compact TiO_2 Layer for Efficient Hole-Blocking in Perovskite Solar Cells. *Appl. Phys. Express* **2014**, *7*, 052301.

DOI: 10.1021/acsami.5b01959
ACS Appl. Mater. Interfaces 2015, 7, 15117−15122

(10) Ke, W.; Fang, G.; Wang, J.; Qin, P.; Tao, H.; Lei, H.; Liu, Q.; Dai, X.; Zhao, X. Perovskite Solar Cell with an Efficient TiO_2 Compact Film. *ACS Appl. Mater. Interfaces* **2014**, *6*, 15959−15965.
(11) Tsai, C. C.; Chu, Y. Y.; Teng, H. A. A Simple Electrophoretic Deposition Method to Prepare TiO_2-B Nanoribbon Thin Films for Dye-Sensitized Solar Cells. *Thin Solid Films* **2010**, *519*, 662−665.
(12) Sakai, N.; Ebina, Y.; Takada, K.; Sasaki, T. Electronic Band Structure of Titania Semiconductor Nanosheets Revealed by Electrochemical and Photoelectrochemical Studies. *J. Am. Chem. Soc.* **2004**, *126*, 5851−5858.
(13) Osada, M.; Sasaki, T. Exfoliated Oxide Nanosheets: New Solution to Nanoelectronics. *J. Mater. Chem.* **2009**, *19*, 2503−2511.
(14) Li, L.; Ma, R. Z.; Ebina, Y.; Fukuda, K.; Takada, K.; Sasaki, T. Layer-by-Layer Assembly and Spontaneous Flocculation of Oppositely Charged Oxide and Hydroxide Nanosheets into Inorganic Sandwich Layered Materials. *J. Am. Chem. Soc.* **2007**, *129*, 8000−8007.
(15) Sugimoto, W.; Terabayashi, O.; Murakami, Y.; Takasu, Y. Electrophoretic Deposition of Negatively Charged Tetratitanate Nanosheets and Transformation into Preferentially Oriented TiO_2(B) Film. *J. Mater. Chem.* **2002**, *12*, 3814−3818.
(16) Kim, S.; Paek, S.; Lee, S. Nanohybrids of Ultrathin Titania Nanosheets and Zinc Oxide Nanoparticles by an Electrostatic Interaction. *J. Nanosci. Nanotechnol.* **2010**, *10*, 60−67.
(17) Burschka, J.; Pellet, N.; Moon, S.-J.; Humphry-Baker, R.; Gao, P.; Nazeeruddin, M. K.; Grätzel, M. Sequential Deposition as a Route to High-Performance Perovskite-Sensitized Solar Cells. *Nature* **2013**, *499*, 316−319.
(18) Shi, J. J.; Luo, Y. H.; Wei, H. Y.; Luo, J. H.; Dong, J.; Lv, S. T.; Xiao, J. Y.; Xu, Y. Z.; Zhu, L. F.; Xu, X.; Wu, H. J.; Li, D. M.; Meng, Q. B. Modified Two-Step Deposition Method for High-Efficiency TiO_2/$CH_3NH_3PbI_3$ Heterojunction Solar Cells. *ACS Appl. Mater. Interfaces* **2014**, *6*, 9711−9718.
(19) Laban, W. A.; Etgar, L. Depleted Hole Conductor-Free Lead Halide Iodide Heterojunction Solar Cells. *Energy Environ. Sci.* **2013**, *6*, 3249−3253.
(20) Snaith, H. J.; Abate, A.; Ball, J. M.; Eperon, G. E.; Leijtens, T.; Noel, N. K.; Stranks, S. D.; Wang, J. T.-W.; Wojciechowski, K.; Zhang, W. Anomalous Hysteresis in Perovskite Solar Cells. *J. Phys. Chem. Lett.* **2014**, *5*, 1511−1515.
(21) Chen, H.-W.; Sakai, N.; Ikegami, M.; Miyasaka, T. Emergence of Hysteresis and Transient Ferroelectric Response in Organo-Lead Halide Perovskite Solar Cells. *J. Phys. Chem. Lett.* **2015**, *6*, 164−169.
(22) Kim, H. S.; Park, N. G. Parameters Affecting I-V Hysteresis of $CH_3NH_3PbI_3$ Perovskite Solar Cells: Effects of Perovskite Crystal Size and Mesoporous TiO_2 Layer. *J. Phys. Chem. Lett.* **2014**, *5*, 2927−2934.
(23) Jena, A. K.; Chen, H.-W.; Kogo, A.; Sanehira, Y.; Ikegami, M.; Miyasaka, T. The Interface between FTO and the TiO_2 Compact layer Can Be One of the Origins to Hysteresis in Planar Heterojunction Perovskite Solar Cells. *ACS Appl. Mater. Interfaces* **2015**, *7*, 9817−9823.

DOI: 10.1021/acsami.5b01959
ACS Appl. Mater. Interfaces 2015, 7, 15117−15122